

Inferring differentiation order in adaptive immune responses from population level data

Alexander S. Miles,* Philip D. Hodgkin,† and Ken R. Duffy‡

August 3, 2021

Abstract

A hallmark of the adaptive immune response is the proliferation of pathogen-specific lymphocytes that leave in their wake a long lived population of cells that provide lasting immunity. A subject of ongoing investigation is when during an adaptive immune response those memory cells are produced. In two groundbreaking studies, Buchholz et al. (Science, 2013) and Gerlach et al. (Science, 2013) employed experimental methods that allowed identification of offspring from individual lymphocytes *in vivo*, which we call clonal data, at a single time point. Through the development, application and fitting of a mathematical model, Buchholz et al. (Science, 2013) concluded that, if memory is produced during the expansion phase, memory cell precursors are made before the effector cells that clear the original pathogen. We sought to determine the general validity and power of the modeling approach introduced in Buchholz et al. (Science, 2013) for quickly evaluating differentiation networks by adapting it to make it suitable for drawing inferences from more readily available non-clonal phenotypic proportion time-courses. We first established the method drew consistent deductions when fit to the non-clonal data in Buchholz et al. (Science, 2013) itself. We fit a variant of the model to data reported in Badovinac et al. (Journal of Immunology, 2007), Schlub et al. (Immunology and Cell Biology, 2010), and Kinjo et al. (Nature Communications, 2015) with necessary simplifications to match different reported data in these papers. The deduction from the model was consistent with that in Buchholz et al. (Science, 2013), albeit with questionable parameterizations. An alternative possibility, supported by the data in Kinjo et al. (Nature Communications, 2015), is that memory precursors are created after the expansion phase, which is a deduction not possible from the mathematical methods provided in Buchholz et al. (Science, 2013). This investigation further supports the value of the approach, though we indicate where published experimental findings run contrary to assumptions underlying the model, which may impact the strength of inferences, and what an alternate model more consistent with recent data might be.

1 Introduction

During an adaptive immune response, a population of naive lymphocytes becomes heterogeneous, containing a population of effector cells that clear the pathogen and then die during the contraction phase, and a population of memory cells that are of a longer lineage. For CD8⁺ T cells, many theories have been proposed for the dynamics of this differentiation. The three primarily championed ones are [1, 16, 4]:

*Hamilton Institute, Maynooth University, Ireland

†Walter and Eliza Hall Institute, Royal Melbourne Hospital, Parkville, Australia and the Department of Medical Biology, The University of Melbourne, Parkville, Australia

‡Hamilton Institute, Maynooth University, Ireland. E-mail: Corresponding ken.duffy@nuim.ie

- **Linear Effector First Model:** Naive cells differentiate into proliferating effector cells. Later in the immune response, these cells differentiate into memory cells or die [19, 13, 23, 15].
- **Linear Memory First Model:** Naive cells differentiate into memory precursor cells that then proliferate, with some differentiating into effector cells. Some time after the expansion phase is completed the effector cells die [3].
- **Bifurcation Model:** Each naive cell has the potential to divide into either effector or memory precursor subsets which then continue to proliferate inheriting their phenotype, and effector cells die after the expansion phase while memory cells remain [5, 14].

These three are non-exhaustive, high-level summaries of a more diverse and subtle set of theories. Provision of a simple classification is further complicated by phenotypic characterization of T cells where there is an overlap between memory and effector functionality and phenotypic markers, sometimes resulting in a sub-category that is referred to as effector memory cells (TEMp, the p standing for precursor) to distinguish them from effector (TEF) and central memory cells (TCMp).

The Linear Effector First Model has a long history and could be considered the traditional view [19, 1]. In 2007, the authors of [5] proposed asymmetric cell division to explain heterogeneity with CD8⁺ T cells, supporting the Bifurcation Model, which won't be considered further here. In 2013, two landmark papers were published [3, 8] that further addressed this question. Both used novel methodologies to determine clonal relationships of cells. In addition, due to the more quantitative nature of their assay, the authors of [3] developed a methodology to fit a memoryless multi-type Bellman-Harris process model [9] to clonal summary statistics of CD8⁺ T cell phenotypes, finding that a quantitative realization of the Linear Memory First Model was the best explanation of their data.

Let us introduce some notation in order to distinguish between the available data sources. For an experiment initiated at time $t = 0$ with n pathogen specific cells, let $c_i^f(t)$ denote the number offspring that are of phenotype $f \in \{1, \dots, F\}$ from an initial transferred naive cell i at time t post infection. The method used in [3] was effectively unique in determining the number of cells of each phenotype that were descendent from an initially naive cell, $c_i^f(t)$, for each i and all $f \in \{\text{TEF}, \text{TEMP}, \text{TCMp}\}$ at $t = \text{day eight post infection}$. We shall refer to this data as being at a clonal level.

A more common experimental set-up [3, 2, 21, 15] provides the fraction of all offspring that are of each phenotype, f , at a given time t ,

$$\rho^f(t) = \frac{\sum_{i=1}^n c_i^f(t)}{\sum_{j=1}^F \sum_{i=1}^n c_i^j(t)},$$

with clonal contributions being indistinguishable. Experiments recording this information are typically performed as a time-course, with cells harvested at distinct days post infection. We shall refer to it as cohort or population level data.

In the present paper, we describe deductions made by taking the modeling framework described in [3] and adapting it to make it suitable for fitting to cohort data. Our aim was to explore the general validity and power of the method for quickly evaluating differentiation networks from simple cohort time series as, unlike clonal data, those data are more readily available. We used the method to interrogate data reported by other authors [2, 21, 15], that employ similar experimental systems to that described in [3].

A high-level summary of the content of this paper is:

1. To adapt the method in [3] for fitting to non-clonal data, we introduce a distinct objective function. On comparing the best parameter fits to six representative models of the 304 considered in the original paper to the time-course cohort data reported in [3] itself, the finding was the same as for the clonal data: that if memory is made during the expansion phase, then the Linear Memory First Model is the best. Moreover, the best-fit parameterization from the cohort data was quantitatively similar to that when fit to clonal data, suggesting consistency of the method.
2. Due to data limitations where fewer phenotypes were identified, for the papers [2, 21, 15] we fit only to two representative differentiation structures: Linear Effector First and Linear Memory First. Naive

application of the methodology to the entire time-course cohort data taken from [15] supported the Linear Effector First Model over the Linear Memory First Model. A more sophisticated application was performed, noting that the number of antigen-specific T cells adoptively transferred in the experiments reported in [15] was significantly higher than in [3], resulting in a curtailed expansion phase. Limiting model fitting to expansion phase only, data from blood and spleen in four papers, [2, 21, 3, 15] all support a Linear Memory First Model in favor of a Linear Effector First Model. Best fit model parameterizations, however, suggest the model is struggling to explain this data.

3. Additional data reported in [15] suggests that the *a priori* assumption underlying the mathematical analysis that memory is created during the expansion phase could be questionable.
4. While the evidence presented here further supports the utility of the method introduced in [3], we indicate some of the discrepancies between its model assumptions and published data, suggesting an alternate model structures that are more consistent with them, which might be of use in future.

2 Experiments and results from relevant papers

Clonal level experiments [3]: The authors performed innovative OT-1 CD8+ T cell adoptive transfer experiments where cell lineage could be determined. Donor mice were engineered to express both CD45 and CD90 markers homozygously, heterozygously or not at all, allowing for nine combinations of markers in total, Fig. 1A. C57BL/6 host mice were chosen from the double heterogeneous marker pool. Recipient mice received a mix of naive OT-1 CD8 T cells that contained one cell from each of the seven uniquely congenically marked donor mice together with 100 cells from one further uniquely marked mouse. As lineage was determined by cell surface markers, clonal cell numbers could be quantitatively evaluated by FACS. The cellular barcoding approach used in the twinned paper [8] was based on DNA tags and their processing via PCR makes that data less suitable for quantitative modeling analysis.

In the experiments reported in [3], the host was infected with 5×10^3 *Listeria monocytogenes*, a pathogenic bacteria, expressing OVA (LM-OVA). At day eight post infection, cells were taken from the spleen, lymph nodes and lungs. The cells were sorted into three phenotypes:

- **TCMp:** CD62L⁺CD27⁺ phenotype.
- **TEMp:** CD62L⁻CD27⁺ phenotype.
- **TEF:** CD62L⁻CD27⁻ phenotype.

Summary statistics from the data collected for these phenotypically defined populations were reported: the average cell count per family, coefficients of variation and correlation coefficients between families for the three phenotypes, Fig. 2A.

Cohort level experiments, [2, 21, 3, 15] Each of these four papers also performed OT-1 CD8+ T cell adoptive transfer experiments, Fig. 1B. In these, cells were not tracked at a clonal level, $\{c_i^f(t)\}$, but at a cohort level $\{\rho^f(t)\}$, via expression of either CD45 or CD90. The host mouse was infected with a pathogen expressing OVA; PR8-OVA in [15] and LM-OVA in the other papers. The reported experiments have cells taken from different organs, spleen, or mesenteric lymph nodes (MLN), at a range of times post infections. In addition, [2, 21] performed experiments with varying number of transferred OT-1 T cells. All of those papers report the percentage of cells that were CD62L⁺ at harvest times.

For cohort spleen and blood data reported in all four papers, at early stages post infection all experiments show an initial large CD62L⁺ population, Fig. 2B, which the authors of [3] associate this with an early memory precursor population while the authors of [15] associate it with cells still being naive. All papers show a decrease in this initial CD62L⁺ proportion, which both [15] and [3] explain is due to the effector pool increasing in size. The paper [15] reports an increase in the percentage of CD62L⁺ by day seven and explains this as cells differentiating into memory cells, whereas the data in [3] continues to show a decrease by day seven.

For experiments with a high number of adoptively transferred cells, [21] and [2] report an earlier expansion peak and a shorter expansion phase. Experiments transferring less than 500 cells had a peak at day seven,

while for experiments transferring 5×10^5 cells the peak immune response occurred at day five. Curtailing the experimental data with higher numbers of adoptively transferred cells to its expansion phase (a method for estimating this time we describe later in the paper) removes much of the later upturn in CD62L proportions, Fig. 2B. Having transferred 5×10^5 cells, the paper [2] estimates the family size increase to be 40 – 400 fold on average at the peak, compared to the estimated 400,000 fold increase on average for the experiment transferring 50 cells.

3 The mathematical model, its adaptation & fit to cohort data reported in [3]

The authors of [3] introduced a collection of memoryless multi-type Bellman-Harris stochastic processes [9] to model the expansion phase of an adaptive immune response based on the following assumptions.

- There are four types of cell: naive, TCMp, TEMp, and TEF.
- There is no cell death during the expansion phase described by the model.
- For each cell type, the lifetime of each cell is an independent and identically exponentially distributed random variable with a cell-type dependent mean.
- At the end of its lifetime, a naive cell differentiates into one of the other cell types.
- TCMp, TEMp, and TEF cells can divide or differentiate, with the each cell's fate determined probabilistically and independently based on a cell-type dependent parameterization.
- Possible differentiation between cell-types is known as a path. Different model types have a different combination of paths between cell types, which can be uni- or bi-directional.
- There must be a direct or indirect path from the naive cell to each cell-type.
- When the combinatorics are all done, the collection of possible paths describes 304 different models with between seven and 12 parameters.

For a given differentiation network and parameterization, the authors of [3] employ a χ^2 distance as a measure of a quality of fit between expected summary statistics and observed summary statistics. Denote the nine observed clonal summary statistics per-phenotype of mean family size, coefficient of variation and Pearson correlation between the phenotypes as $\hat{x} = (\hat{x}_1, \dots, \hat{x}_9) \in \mathbb{R}^9$, and their equivalent expected values for a given model plus parameterization, θ , as $\bar{x}(\theta) \in \mathbb{R}^9$. With experimental uncertainty of each observation, \hat{x}_i , estimated by bootstrap approximation as $\hat{\sigma}_i$, the χ^2 distance between models and observations is computed to be

$$d_1(\hat{x}, \bar{x}(\theta)) = \sum_{i=1}^9 \frac{(\hat{x}_i - x_i(\theta))^2}{\hat{\sigma}_i^2}.$$

For each of the 304 possible models, the best-fit parameterization, $\theta^* = \arg \inf_{\theta} d_1(\hat{x}, \bar{x}(\theta))$, was numerically identified and more involved models were penalised via Akaike Information Criterion (AIC). One of the two best fits over all 304 possible differentiation networks was a linear differentiation pathway with memory cells appearing before effector cells (the second model was as the first, but with an additional 10% chance for naive to skip the TCMp stage of the path).

We wished to determine the method's consistency when fitting the model class described in [3] to the time-course cohort data $\{\rho^f(t) : t = \text{day } 1, 2, 3, 4, 6, 8\}$, described in that paper rather than to the clonal data $\{c_i^f(t) : t = \text{day } 8\}$ as the authors had originally done. To do so, we replaced the clonal summary statistics with $\hat{y} = (\hat{y}_1, \dots, \hat{y}_{19})$ where \hat{y}_1 is the average family size at the peak and y_2, \dots, y_{19} are the 18 measured proportions of phenotypes observed at different times post infection. We denote $\hat{\sigma}_i$ as the sample error of the statistic

\hat{y}_i . In the case of the average family size, the SEM was approximated by summing together the SEMs of the phenotypic components. Thus, we use the formulae

$$d_2(\hat{y}, \bar{y}(\theta)) = \sum_{i=1}^{19} \frac{(\hat{y}_i - y_i(\theta))^2}{\hat{\sigma}_i^2}.$$

to measure the distance between expected and observed cohort statistics.

We numerically identified the best fit parameterization of the model for six representative differentiation pathways, Fig. 3A, of the 304 considered in [3]. These six were chosen since they include one of the two best fit models and were sufficient to recreate the most significant results reported in [3]. We label the six models by:

- **Model 1:** Naive \rightarrow CD62L⁺CD27⁺ \rightarrow CD62L⁻CD27⁺ \rightarrow CD62L⁻CD27⁻.
- **Model 2:** Naive \rightarrow CD62L⁺CD27⁺ \rightarrow CD62L⁻CD27⁻ \rightarrow CD62L⁻CD27⁺.
- **Model 3:** Naive \rightarrow CD62L⁺CD27⁻ \rightarrow CD62L⁺CD27⁺ \rightarrow CD62L⁻CD27⁻.
- **Model 4:** Naive \rightarrow CD62L⁺CD27⁻ \rightarrow CD62L⁻CD27⁻ \rightarrow CD62L⁺CD27⁺.
- **Model 5:** Naive \rightarrow CD62L⁻CD27⁻ \rightarrow CD62L⁺CD27⁺ \rightarrow CD62L⁺CD27⁻.
- **Model 6:** Naive \rightarrow CD62L⁻CD27⁻ \rightarrow CD62L⁻CD27⁺ \rightarrow CD62L⁺CD27⁺.

Model 1 is one of the two original best fitting models reported in [3]. As these models all have the same number of parameters, we do not need to consider penalization by AIC. Due to less extensive data in [2, 21, 15], later we will reduce the set model further to consider just two competing models, Memory (CD62L⁺) First and Effector (CD62L⁻) First, Fig. 3B.

The model in [3] has four cell types, but only reports data for three phenotypes and no statistics for naive cells are presented. This could be interpreted two ways, either naive cells have been excluded from the data, or they were included in the count of one of the other phenotypes. We note that [3] define naive cells as CD62L⁺CD27⁺ ([3] Supplementary Fig. 3), but with a different gating strategy than used for the classification of other cell types ([3] Supplementary Fig. 22). For the analysis here, we assume that naive cells are included in the TCMp count reported in [3].

When applied to the time-course cohort data reported in [3], we found that Model 1, Memory First, to be the best fit, consistent with the original deduction from fitting to clonal data, Fig. 4A. Notably, the parameterization for the best fitting model was remarkably similar for five parameters out of six, as shown in Fig. 4B. Fitting to either data-set is consistent with an increase in the division rate as cells differentiate from memory to effector cells, as also reported in [3]. The difference in the parameter λ_N , which parameterizes the lifetime of naive cells, could be explained by the fact that the adjusted method compares the sum of proportions of naive and TCMp cells to one statistic, the proportion of CD62L⁺CD27⁺ cells, and is not able to discriminate between their separate contributions. These results suggest that, for this model, fitting to time-course cohort data with an average family size is a reasonable alternative to fitting to clonal data of mean count of cells, variances and covariances.

4 Adaptation and application to cohort data from [2, 21, 15]

Adaptation. As data from other papers we wish to analyze, [2, 21, 15], did not include all of the information as [3] it was necessary to use a modified scheme. In some cases, average family size or SEM information was not given. All four papers provide the proportion of CD62L⁺ cells, but some do not report CD27 data. Thus we define a new set of models that do not distinguish between CD27⁻ and CD27⁺ cells so that we can fit the observed statistics without this information. We change the assumption that there are four underlying cell types: naive, TCMp, TEMp and TEF used in [3], to three cell types: naive, memory and effector cells. Thus the phenotypes are:

- **Naive and memory cells:** CD62L⁺ phenotype.

- **Effector cells:** CD62L⁻ phenotype.

We label the two versions of these models as:

- **Linear Memory First Model** differentiation path: Naive \rightarrow CD62L⁺ \rightarrow CD62L⁻.
- **Linear Effector First Model** differentiation path: Naive \rightarrow CD62L⁻ \rightarrow CD62L⁺.

It is estimated that a mouse has 100–1000 cells capable of responding to any specific antigen, meaning large adoptive transfers such as 10^6 used in [15] dwarf the endogenous response [2]. The papers [2, 21] establish that increased transfer size leads to an earlier peak response. We used log-linear fitting to approximate the relationship between the number of transferred cells and the day of peak response, Fig. 5A. For an experiment transferring 107 cells, as described in [3], we estimate the peak to be at day between seven and eight. For an experiment transferring 10^6 cells, as described in [15], we estimate the peak day to be between day four and five. We proceed with the assumption in [3] that the expansion phase in that system continues until day eight.

The χ^2 objective function employed by [3] uses estimates of the sample variance, $\hat{\sigma}_i^2$, for each observed statistic. There is not, however, sufficient data reported to make the bootstrapping calculation for the SEM of [15] data. As a result we needed to modify the weighting in the objective function so it was not dependent on this missing information. This weighting also has to manage the fact that an average family size is on a different scale than a proportional statistic. Let us suppose we have an observed average family size denoted as \hat{y}_1 and k statistics observed of proportional phenotypes at different times denoted as $\hat{y}_2, \dots, \hat{y}_{k+1}$. The objective function we applied was a weighted mean squared error defined by

$$d_3(\hat{y}, \bar{y}(\theta)) = \frac{(\hat{y}_1 - y_1(\theta))^2}{\hat{y}_1^2} + \sum_{i=2}^k (\hat{y}_i - y_i(\theta))^2.$$

That is, we use another weighted mean squared error where we only divide one of the sum's elements by the respective observed statistic squared, the observed populations at day eight post infection. This weighting is required to ensure that the population statistic does not disproportionately influence the objective function, as the population scales exponentially over time while the proportional statistics do not.

The methodology of fitting models to observed cohort data requires an estimate of the average family size at peak immune response in order for models to scale correctly, however this data is not reported in [15]. The authors of [21] provide a methodology for estimating the difference in the average number of divisions transferred OT-1 CD8+ T cells have made by the time of peak response between two experiments. We adopt and extend this method to estimate average family size at peak. We fit a log linear relationship to estimate the percentage of OT-1 cell at peak of the immune response for different adoptive transfer amounts, Fig. 5B. We also make the assumption that the total number lymphocytes (OT-1 and endogenous) at the peak immune response is the same across all experiments, an assumption supported by spleen data in [21]. Spleen counts reported in [2] suggest this may not always be the case, particularly for low transfer numbers. Finally we assume that the average family size reported in [3] is representative. Combing these assumptions allowed us to derive the average family size for a given adoptive transfer of OT-1 cells, Fig. 5C. The log-linear assumption is used for simplicity, but predicts negative growth for low numbers of OT-1 cells, and so can only be useful above a threshold.

This scheme indicates that with a transfer of 1×10^2 cells, as in [3], each clone results in an average of nine more divisions than the clones in a transfer of 1×10^6 cells, as in [15]. This scales roughly with that estimated in [21] that a transfer of 3.2×10^3 cells results in five more divisions than a 4×10^5 transfer. We calculate that in the experiment reported in [15] we would expect 23 cells per family (four to five average divisions) at the peak of around day 4.5. This is reasonable when compared to data in [2], which reported that there is only a 13 fold increase in total OT-1 proportion at peak for a 10^4 fold increase in precursor transfer. While relative numbers are comparable, large discrepancies in reported data for absolute cell counts highlight caveats with these estimates. On transferring 10^2 cells, [3] reports an average peak family size of 15k, while [2] gives a 400k estimate for 50 cells transferred. Our estimate for the total number of lymphocytes in a mouse, calculated from the value reported in [3], is four fold lower than that [21] reported in the spleen. Because of the fragility of this calculation, we performed a sanity check which established there was no significant impact (data not shown).

Application. When fitting to all the data in [15] up to day eight post infection, contrary to the deduction in [3], the method indicated that the Linear Effector First Model provided the better fit, Fig. 6A. The Linear Effector First Model was also the best fit for the experiments in [21] with high adoptive transfer numbers. For experiments with lower numbers of adoptively transferred cells, the deduction flipped and the Linear Memory first model was the best fit. Thus, when fitting without adjusting for the number of cell adoptively transferred, we found contradictory results.

We restricted the data from these papers to the estimated expansion phase. Curtailed data with less than four data points was not considered. For all other data sets, the Linear Memory First Model provided the best fit, Fig. 6B. On examination, however, all of best fits, had biologically implausible parameterizations, with naive cell average lifetimes taking values far over 10 days, with the one exception of the Memory First model fitting to [3] data. This is at odds with data showing that, even for high adoptive transfers, less than 0.1% of the OT-1 population comprised unrecruited cells [21], and data from [15] showing that while no cells had divided on day two post infection the majority were preparing to divide. We therefore further adapted the method, re-performing the analysis, but upper bounding parameters so that average cell lifetime is five days or less. When fitting with this adjustment, the Linear Memory First Model still provided the best fit to all the curtailed data sets, but the result was stronger, with the Linear Effector First Model failing to give a good explanation for the data in [3, 15], Fig. 6C. This result suggested that under the assumptions of the model there was no biologically plausible good fit for the Linear Effector First Model when fit to either data set. We applied the fitting method to blood data from [2] which was not included in the main analysis, and this also returned a Memory First model as the best fit, Fig. 6D. We also applied the method to MLN data reported in [15], which, in contrast to the other data, returned the Linear Effector First Model as the best fit. The MLN data, however, may not be appropriate for this analysis, due to the high levels of migration.

The method chose boundary values for at least one parameter in all cases except when fitting the Linear Memory First Model to [3] data, Fig. 7. In addition, some models predicted little memory, primarily fitting the CD62L⁺ portion with naive and effector cells, as was the case with the Effector First Model fitted to [15]. This suggested that the model may not be sophisticated enough or did not have enough data to fit to. An alternative explanation could come from other [15] results, which showed a homogeneous population effectors on day four post infection make way for two homogeneous groups of effectors and memory cells on day seven. With the insight that day seven is after the expansion phase in the experimental setup described in [15], this result suggests the possibility that memory may appear after the strictly exponential expansion phase considered by the model in [3] has come to an end.

5 Discussion

The evidence presented here suggests that the modeling methodology introduced in [3] to discriminate between differentiation pathways, originally implemented to fit to clonal data, is robust in its deductions when modified to fit to more readily available time-course non-clonal data. Robustness is a key advantage of the approach for quickly evaluating differentiation networks.

We acknowledge that our application of the model to published data has several limitations beyond the original: we considered a much more limited collection of linear-only paths; we had to collapse phenotypic definitions due to not having CD27 measurements; we extracted data from papers directly from graphs; we employed an adapted method for estimating day of peak immune response, and average family size.

Despite all of those considerations, the model provided a robust outcome when fit to the non-clonal cohort time-course published in [3]. Once day of peak response was taken into account, it produced consistent deductions, that within this modeling framework Memory First provides the best fit, across a range of data from other papers [2, 21, 15]. When inappropriately fit to time-courses that extend beyond the expansion phase, interestingly it supported the Effector First Model in some cases, which is more consistent with other data in [15].

As with any modeling framework, there are, of course, caveats in the strength of the conclusions drawn from it. Presumably due to the inherently limited nature of the *in vivo* data being fit, several modeling assumptions were made in [3] that keep the computational model tractable and parameters identifiable, but

some of which are inconsistent with published experimental data. As more sophisticated tracking of cell familial fates and information on physiological constraints around lineage transitions develops, we anticipate that ultimately other mathematical models will be employed that are built on that knowledge. For illustration, we attempt to highlight where those assumptions may influence the deductions of the present study.

The model's remit is exclusively an expansion phase with no death and strictly exponentially growing populations. As a result, the method cannot be reasonably expected to draw inferences on differentiation if it occurs as motivation to divide is petering out.

The fundamental unit of autonomous randomness in the model is the cell: each cell is born afresh, independently selecting its lifetime and fate in a cell-type dependent fashion. The data in both [3, 8] illustrate a strong familial influence, with some clones expanding dramatically more than others. Controlled *in vitro* experiments have established significant elements of clonal dependency [16], notably in burst size [17, 12], while *in vivo* data using the cell cycle reporter Fucci [20] has established that during an adaptive immune response cells drop out of cycle as early as day four and the number of non-dividing cells progressively increases with time [18]. Thus, to retain simplicity and identifiability, an alternative view, taking to account these experimental features would posit that the ultimate clone burst size is randomized between families, and that the slowing in proliferation rate noted by the memory first model, Fig. 4B and Fig. 7B, is created by non-dividing memory cells diluting the average division time of the OT-1 populations being measured.

The use of an exponential distribution for the lifetime distribution ensures that the multi-type Bellman-Harris process is Markovian, and facilitates the use of non-asymptotic values in model fitting. Due to the minimum time needed to synthesize DNA, there is always a lower-bound on division times and it has been long since known that for lymphocytes, at least *in vitro*, the exponential does not offer a good description of the distribution of division times and a right skewed distribution is more appropriate [22, 6, 11, 10, 7]. Thus, while cohort and clonal data yielded the same deductions in our analysis, only experiments looking deeper than the population level can shed light on the validity of the modeling assumptions used for inference.

Whether a model built taking these assumptions into account would lead to distinct deductions is unclear. What is clear is that, within the confines of the assumptions underlying it, the model introduced in [3] provides a method for quickly evaluating differentiation networks, even for cohort level data.

Acknowledgement. The work of A.M. and K.R.D. was supported by Science Foundation Ireland Grant 12IP1263. This work was supported by the National Health and Medical Research Council of Australia via Project Grant 1010654, Program Grant 1054925 and a fellowship to P.D.H. as well as an Australian Government National Health and Medical Research Council Independent Research Institutes Infrastructure Support Scheme Grant 361646.

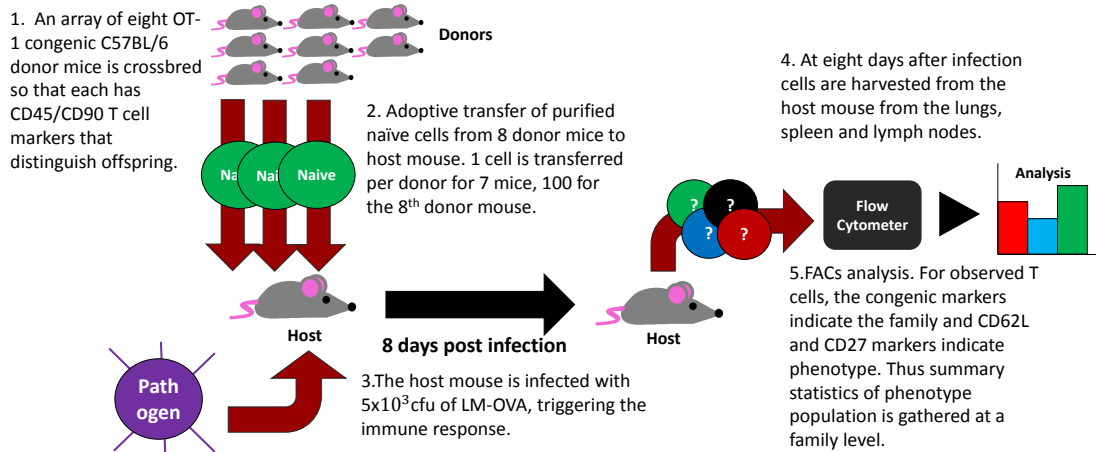
References

- [1] Rafi Ahmed, Michael J. Bevan, Steven L. Reiner, and Douglas T. Fearon. The precursors of memory: models and controversies. *Nature Reviews Immunology*, 9(9):662–668, 2009.
- [2] Vladimir P. Badovinac, Jodie S. Haring, and John T. Harty. Initial T cell receptor transgenic cell precursor frequency dictates critical aspects of the CD8+ T cell response to infection. *Immunity*, 26(6):827–841, 2007.
- [3] Veit R. Buchholz, Michael Flossdorf, Inge Hensel, Lorenz Kretschmer, Bianca Weissbrich, Patricia Gräf, Admar Verschoor, Matthias Schiemann, Thomas Höfer, and Dirk H. Busch. Disparate individual fates compose robust CD8+ T cell immunity. *Science*, 340(6132):630–635, 2013.
- [4] Veit R. Buchholz, Ton N. M. Schumacher, and Dirk H. Busch. T cell fate at the single-cell level. *Annual review of immunology*, 34:65–92, 2016.
- [5] John T. Chang, Vikram R. Palanivel, Ichiko Kinjyo, Felix Schambach, Andrew M. Intlekofer, Arnob Banerjee, Sarah A. Longworth, Kristine E. Vinup, Paul Mrass, Jane Oliaro, Nigel Killeen, Jordan S. Orange, Sarah M. Russell, Wolfgang Weninger, and Steven L. Reiner. Asymmetric T lymphocyte division in the initiation of adaptive immune responses. *Science*, 315(5819):1687–1691, 2007.

- [6] Mark R. Dowling, Andrey Kan, Susanne Heinzel, Jie H. S. Zhou, Julia M. Marchingo, Cameron J. Wellard, John F. Markham, and Philip D. Hodgkin. Stretched cell cycle model for proliferating lymphocytes. *Proceedings of the National Academy of Sciences*, 111(17):6377–6382, 2014.
- [7] Ken R. Duffy, Cameron J. Wellard, John F. Markham, Jie H. S. Zhou, Ross Holmberg, Edwin D. Hawkins, Jhagvaral Hasbold, Mark R. Dowling, and Philip D. Hodgkin. Activation-induced B cell fates are selected by intracellular stochastic competition. *Science*, 335(6066):338–341, 2012.
- [8] Carmen Gerlach, Jan C. Rohr, Leïla Perié, Nienke van Rooij, Jeroen W. J. van Heijst, Arno Velds, Jos Urbanus, Shalin H. Naik, Heinz Jacobs, Joost B. Beltman, Rob J. de Boer, and Ton N. M. Schumacher. Heterogeneous differentiation patterns of individual CD8+ T cells. *Science*, 340(6132):635–639, 2013.
- [9] Theodore E Harris. *The Theory of Branching Processes*. The RAND Corporation, 1964.
- [10] E. D. Hawkins, J. F. Markham, L. P. McGuinness, and P. D. Hodgkin. A single-cell pedigree analysis of alternative stochastic lymphocyte fates. *Proceedings of the National Academy of Sciences*, 106(32):13457–13462, 2009.
- [11] E. D. Hawkins, M. L. Turner, M. R. Dowling, C. van Gend, and P. D. Hodgkin. A model of immune regulation as a consequence of randomized lymphocyte division and death times. *Proceedings of the National Academy of Sciences*, 104(12):5032–5037, 2007.
- [12] Susanne Heinzel, Tran Binh Giang, Andrey Kan, Julia M Marchingo, Bryan K Lye, Lynn M Corcoran, and Philip D Hodgkin. A Myc-dependent division timer complements a cell-death timer to regulate T cell and B cell responses. *Nature Immunology*, 18:96–103, 2017.
- [13] Joshyi Jacob and David Baltimore. Modelling T-cell memory by genetic marking of memory T cells in vivo. *Nature*, 399:593–597, 1999.
- [14] Carolyn G. King, Sabrina Koehli, Barbara Hausmann, Mathias Schmalzer, Dietmar Zehn, and Ed Palmer. T cell affinity regulates asymmetric division, effector cell differentiation, and tissue pathology. *Immunity*, 37(4):709–720, 2012.
- [15] Ichiko Kinjyo, Jim Qin, Sioh-Yang Tan, Cameron J. Wellard, Paulus Mrass, William Ritchie, Atsushi Doi, Lois L. Cavanagh, Michio Tomura, Asako Sakaue-Sawano, Osami Kanagawa, Atsushi Miyawaki, Philip D. Hodgkin, and Wolfgang Weninger. Real-time tracking of cell cycle progression during CD8+ effector and memory T-cell differentiation. *Nature Communications*, 6:6301 EP –, 2015.
- [16] Fabrice Lemaître, H el ene D Moreau, Laura Vedele, and Philippe Bousso. Phenotypic CD8+ T cell diversification occurs before, during, and after the first T cell division. *The Journal of Immunology*, 191(4):1578–1585, 2013.
- [17] J. M. Marchingo, G. Prevedello, A. Kan, S. Heinzel, P. D. Hodgkin, and K. R. Duffy. T-cell stimuli independently sum to regulate an inherited clonal division fate. *Nature Communications*, 7:13540, 2016.
- [18] Julia M. Marchingo, Andrey Kan, Robyn M. Sutherland, Ken R. Duffy, Cameron J. Wellard, Gabrielle T. Belz, Andrew M. Lew, Mark R. Dowling, Susanne Heinzel, and Philip D. Hodgkin. Antigen affinity, costimulation, and cytokine inputs sum linearly to amplify T cell expansion. *Science*, 346(6213):1123–1127, 2014.
- [19] Joseph T. Opferman, Bertram T. Ober, and Philip G. Ashton-Rickardt. Linear differentiation of cytotoxic effectors into memory T lymphocytes. *Science*, 283(5408):1745–1748, 1999.
- [20] Asako Sakaue-Sawano, Hiroshi Kurokawa, Toshifumi Morimura, Aki Hanyu, Hiroshi Hama, Hatsuki Osawa, Saori Kashiwagi, Kiyoko Fukami, Takaki Miyata, Hiroyuki Miyoshi, Takeshi Imamura, Masaharu Ogawa, Hisao Masai, and Atsushi Miyawaki. Visualizing spatiotemporal dynamics of multicellular cell-cycle progression. *Cell*, 132(3):487–498, 2008.
- [21] Timothy E. Schlub, Vladimir P. Badovinac, Jaime T. Sabea, John T. Harty, and Miles P. Davenport. Predicting CD62L expression during the CD8+ T cell response in vivo. *Immunology and Cell Biology*, 88(2):157–164, 2010.

- [22] J. A. Smith and L. Martin. Do cells cycle? *Proceedings of the National Academy of Sciences*, 70(4):1263–1267, 1973.
- [23] E. John Wherry, Volker Teichgräber, Todd C. Becker, David Masopust, Susan M. Kaech, Rustom Antia, Ulrich H. von Andrian, and Rafi Ahmed. Lineage relationship and protective immunity of memory CD8 T cell subsets. *Nature Immunology*, 4:225–234, 2003.

A.



B.

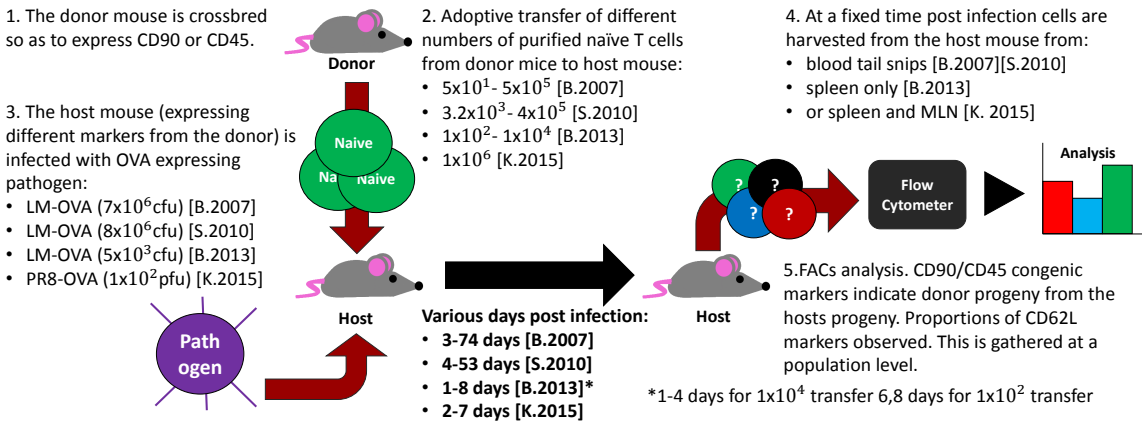
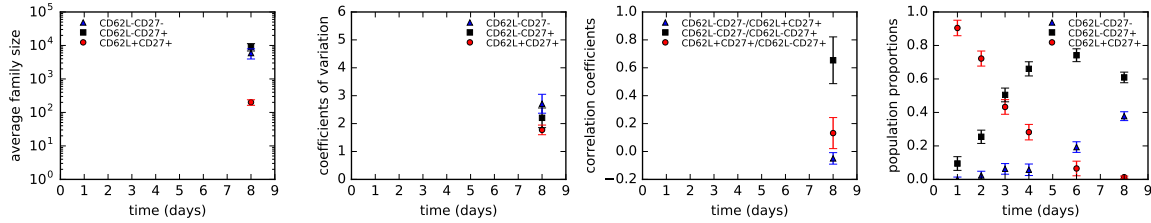


Figure 1. Summary adoptive transfer experiments described in [2, 21, 3, 15]. (A) Experiments described in [3] determine the number of cells per OT-1 CD8+ T cell clone at day eight. (B) All four papers describe similar OT-1 CD8+ T cell adoptive transfer experiments, where cohort data is reported for a time-course of days post infection. The number of cells adoptively transferred varies between papers.

A.



B.

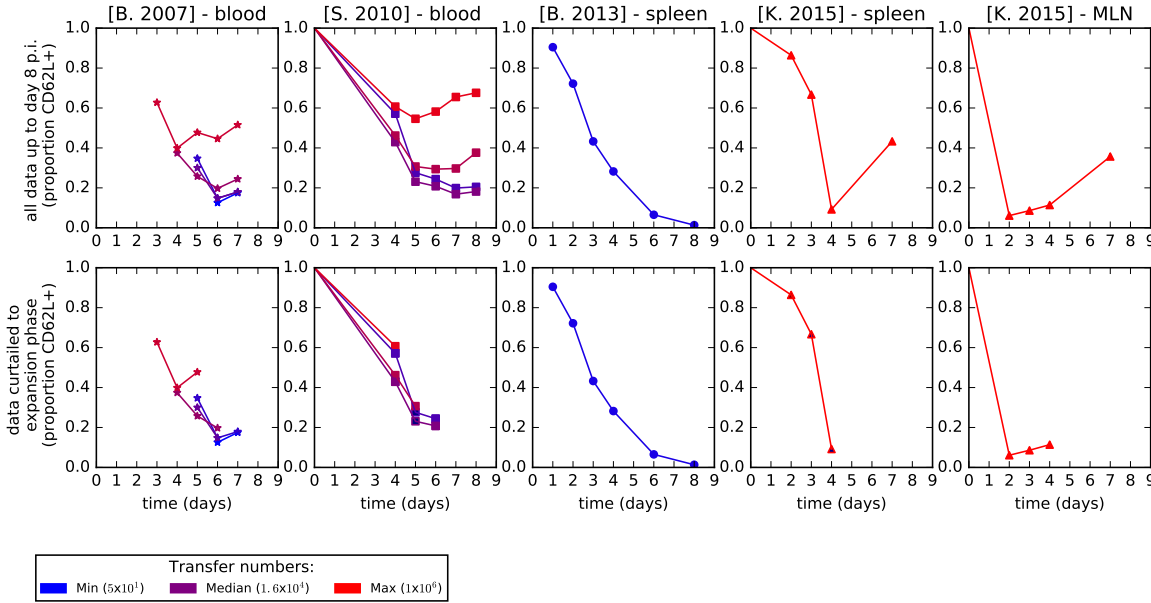


Figure 2. Experimental data from [2, 21, 3, 15]. Data manually extracted from graphs in those papers. (A, left three graphs) Results from the clonal experiment described in [3], showing average family size, coefficients of variation and correlations for different phenotypes populations. (A, rightmost graph) Proportional phenotype results from the cohort experiment. (B) Comparing the CD62L⁺ proportions from the four papers reporting cohort data. The top row shows all reported data up to day eight post infection. The bottom row shows the data when curtailed to the estimated expansion phase, which is shortened due to high adoptive transfer cell numbers.

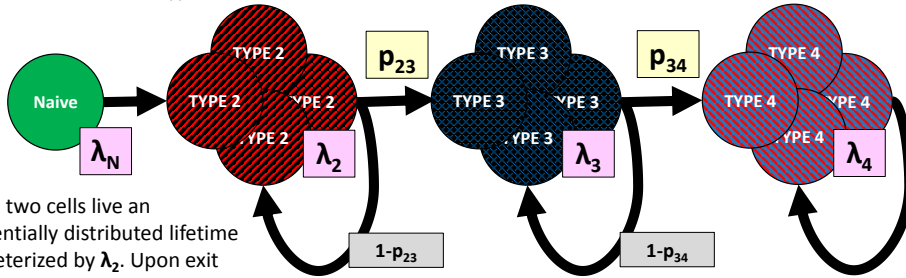
A.

1. Naïve cells live an exponentially distributed lifetime parameterized by λ_N . Upon exit from this state, naïve cells become one cell of type two.

3. Type three cells live an exponentially distributed lifetime parameterized by λ_3 . Upon exit from this state, type three cells differentiate into one cell of type four with probability p_{34} or divide into two type three cells with probability $1-p_{34}$.

2. Type two cells live an exponentially distributed lifetime parameterized by λ_2 . Upon exit from this state, type two cells differentiate into one cell of type three with probability p_{23} or divide into two type two cells with probability $1-p_{23}$.

4. Type four cells live an exponentially distributed lifetime parameterized by λ_4 . Upon exit from this state, type four cells always divide into two type four cells.



B.

1. Naïve cells live an exponentially distributed lifetime parameterized by λ_N . Upon exit from this state, naïve cells become one cell of type two.

3. Type three cells live an exponentially distributed lifetime parameterized by λ_3 . Upon exit from this state type three cells always divide into two type three cells.

2. Type two cells live an exponentially distributed lifetime parameterized by λ_2 . Upon exit from this state, type two cells differentiate into one cell of type three with probability p_{23} or divide into two type three cells with probability $1-p_{23}$.

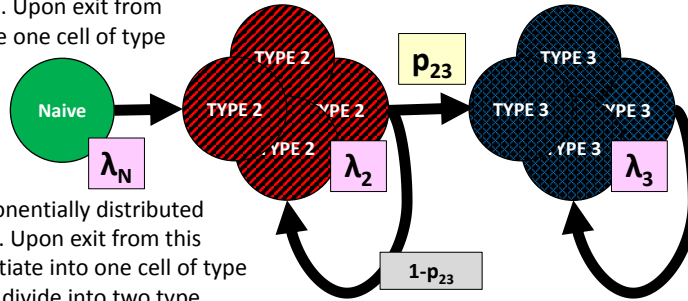


Figure 3. Linear differentiation models considered here. (A) These linear models are a subset of the 304 multi-type Bellman-Harris processes modeled by [3]. Each of the six models has six parameters, $(\lambda_N, \lambda_2, \lambda_3, \lambda_4, p_{23}, p_{34})$. (B) Simplified linear models, with the observed phenotypes reduced from three ($CD62L^+CD27^+$, $CD62L^+CD27^-$, $CD62L^-CD27^-$) to two ($CD62L^+$, $CD62L^-$) and cell types reduced from four to three. The simplified model has four parameters, $(\lambda_N, \lambda_2, \lambda_3, p_{23})$.

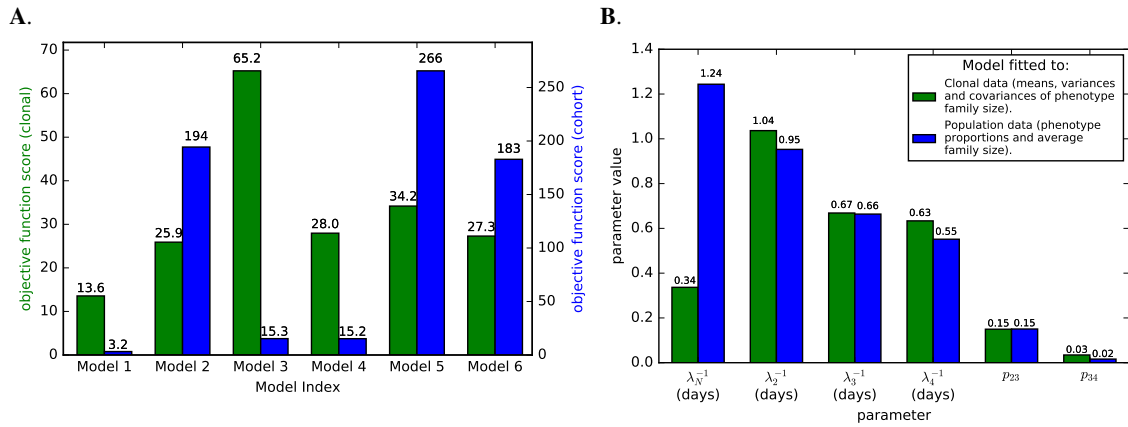


Figure 4. Results from fitting the linear models to clonal data, as in the original method, or cohort data from [3]. (A) Objective function values for the best fitting parameterization of each model, where smaller values indicate a better fit. (B) Best fitting parameterization for Model 1, where λ_2 corresponds to CD62L⁺CD27⁺ (TCMp), λ_3 to CD62L⁻CD27⁺ (TEMp), λ_4 to CD62L⁻CD27⁻ (TEF), p_{23} to the probability that a TCMp cell becomes a TEMp cell and p_{34} to the probability that a TEMp cell becomes a TEF cell.

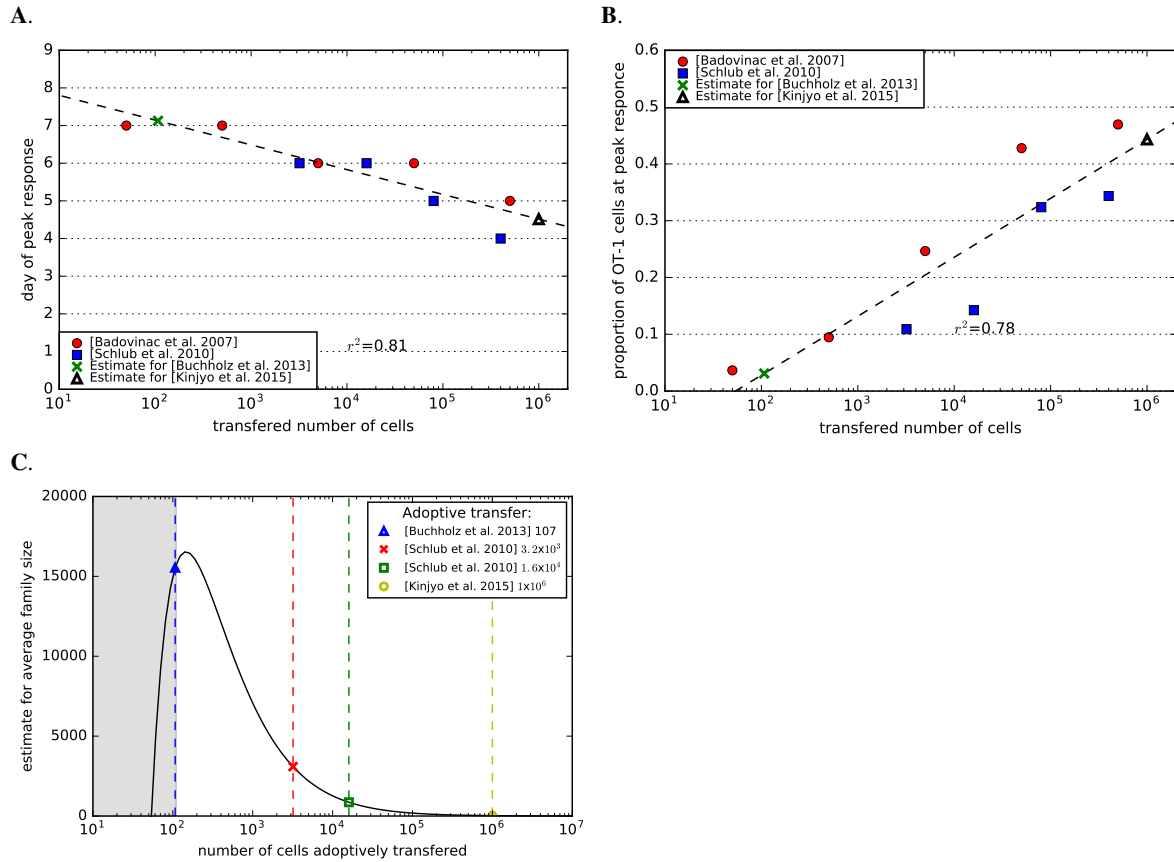


Figure 5. Estimates of the day of peak response and average family size as a function of the number of adoptively transferred cells, using data from [2, 21]. (A) Log-linear regression was used to find an estimate for the day of peak response (y co-ordinate) from the number of adoptively transferred cells (x co-ordinate) reported in [15] and [3]. (B) as in A but estimating proportion of OT-1 cells of lymphocytes at peak. (C) Estimate of average family size at peak for given number of adoptively transferred cells. For low numbers of transferred cells (<100) the estimate is not good.

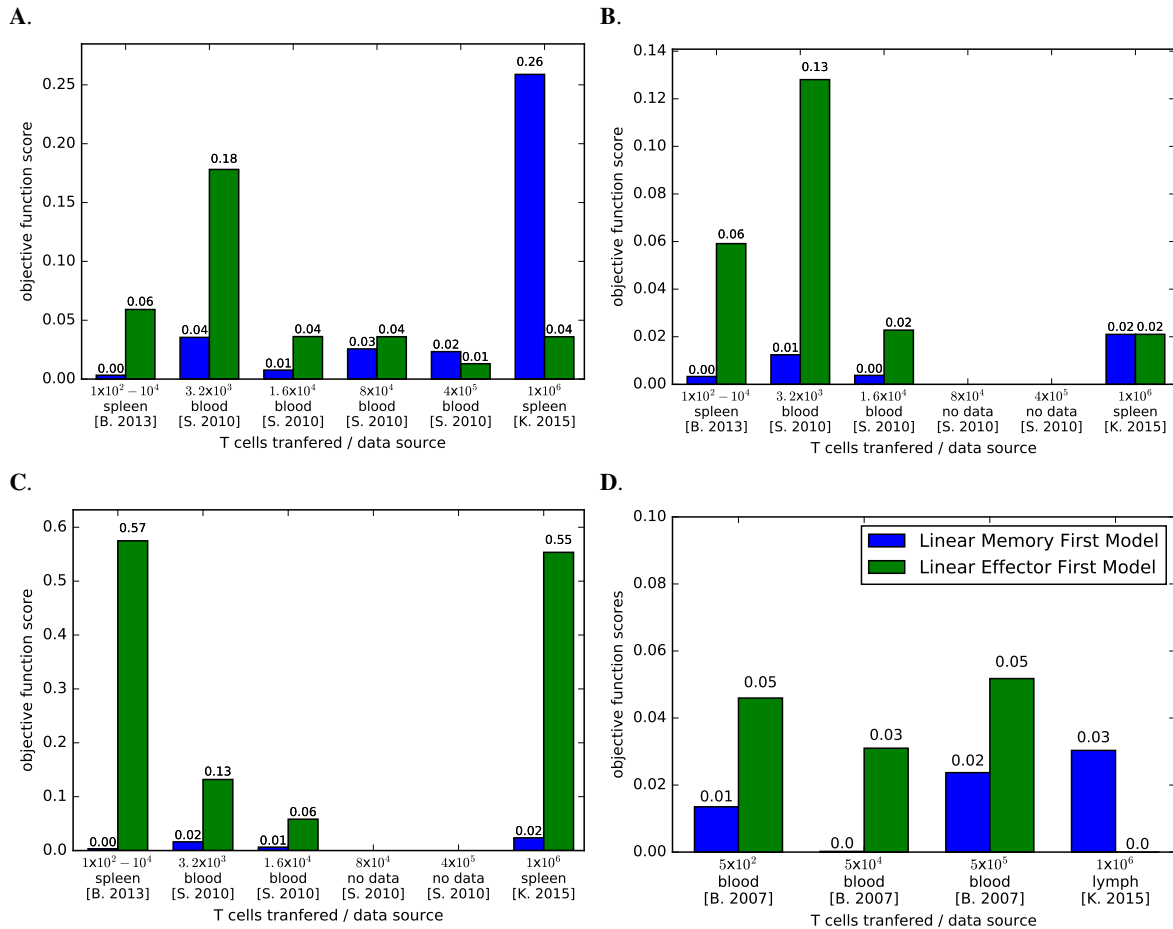


Figure 6. The objective function value for the two simplified linear models for the best parameterizations when fitting cohort statistics and average family size. Smaller numbers indicate a better fit. Fits only done when data sets had four or more data points. (A) Fitted to all reported data up to day eight post infection. (B) As in A, but curtailing data to the estimated expansion phase. (C) As in B, but with the average cell lifetime limited to being below five days. (D) as in C, but fit to additional data sources.

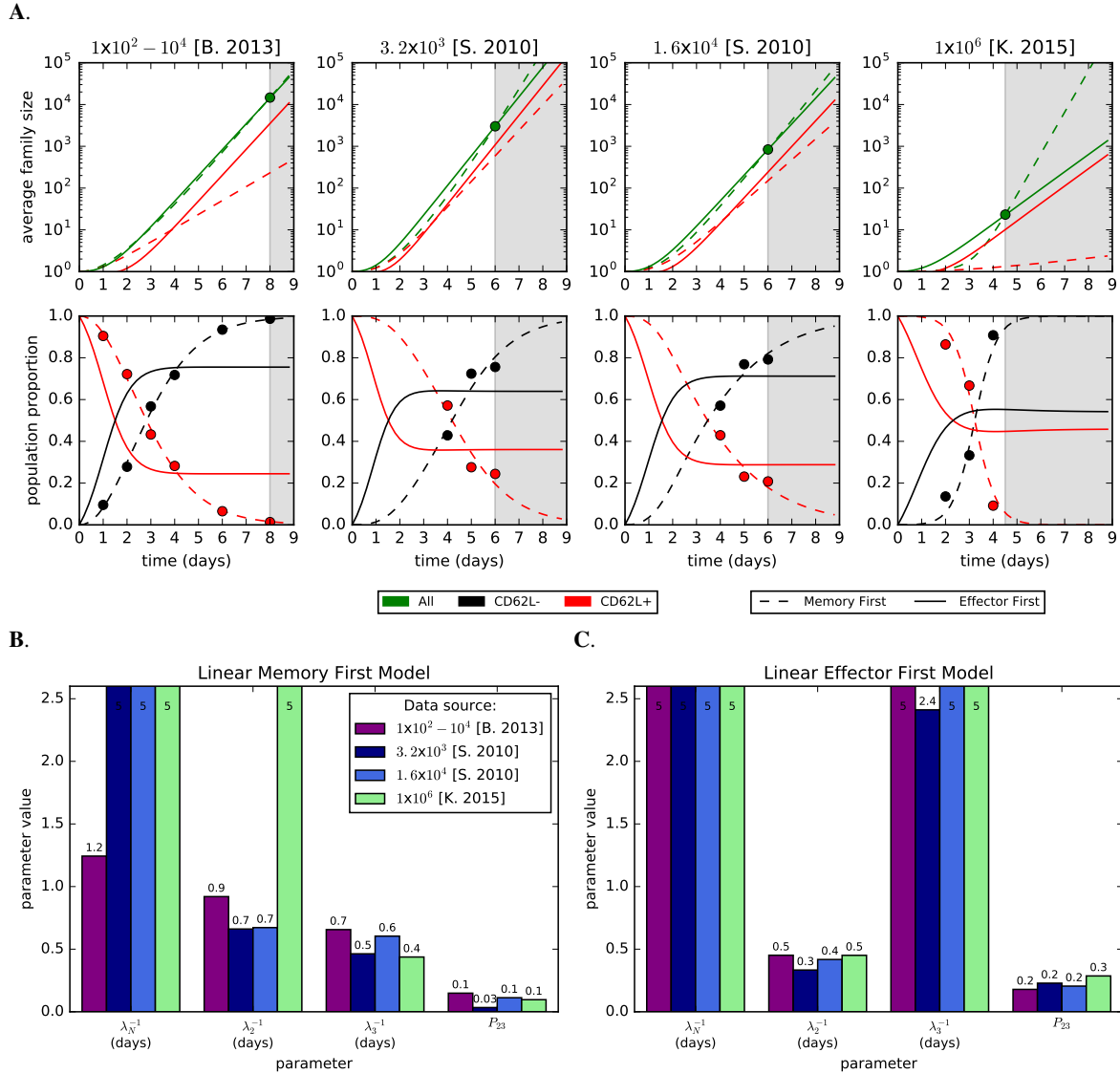


Figure 7. Statistics and parameterization for the best fitting models for cohort data from [3, 15, 21] as in Fig. 6C. (A) Dashed lines show the Linear Memory First Model predicted statistics, solid lines show the Linear Effector First Model predicted statistics, dots show experimental data fitted to and the grey area shows the estimated time after the expansion phase has ended. (B) Parameters for the best fit Linear Memory First Model. (C) Parameters for the best fit Linear Effector First Model.